ADVANCED BIOLOGY
www.advanced-bio.com

A Shearless Microfluidic Device Detects a Role in Mechanosensitivity for AWC^{ON} Neuron in *Caenorhabditis elegans*

Davide Caprini, Silvia Schwartz, Enrico Lanza, Edoardo Milanetti, Valeria Lucente, Giuseppe Ferrarese, Letizia Chiodo, Martina Nicoletti, and Viola Folli*

AWC olfactory neurons are fundamental for chemotaxis toward volatile attractants in *Caenorhabditis elegans*. Here, it is shown that AWC^{ON} responds not only to chemicals but also to mechanical stimuli caused by fluid flow changes in a microfluidic device. The dynamics of calcium events are correlated with the stimulus amplitude. It is further shown that the mechanosensitivity of AWC^{ON} neurons has an intrinsic nature rather than a synaptic origin, and the calcium transient response is mediated by TAX-4 cGMP-gated cation channel, suggesting the involvement of one or more "odorant" receptors in AWC^{ON} mechanotransduction. In many cases, the responses show plateau properties resembling bistable calcium dynamics where neurons can switch from one stable state to the other. To investigate the unprecedentedly observed mechanosensitivity of AWC^{ON} neurons, a novel microfluidic device is designed to minimize the fluid shear flow in the arena hosting the nematodes. Animals in this device show reduced neuronal activation of AWC^{ON} neurons. The results observed indicate that the tangential component of the mechanical stress is the main contributor to the mechanosensitivity of AWC^{ON}. Furthermore, the microfluidic platform, integrating shearless perfusion and calcium imaging, provides a novel and more controlled solution for in vivo analysis both in micro-organisms and cultured cells.

1. Introduction

Caenorhabditis elegans, a microscopic transparent soil nematode with 302 neurons and a well-defined neural connectivity, is one of the most popular bio-platform to study the functioning of nervous systems. Despite its anatomical simplicity, *C. elegans* displays an impressively rich repertoire of simple and more complex behaviors arising from a large variety of different sensory cues, such as smell, taste, touch, oxygen level, and temperature.[1–3] The chemosensory network, comprising ≈34 chemosensory neurons, is one of the most studied circuits in *C. elegans* for the richness of its functioning despite the low number of neurons involved.[3–5]

By using genetically encoded calcium indicators, it is possible to record neuronal activity at single-cell resolution in response to a specific chemical stimulus.[6] Microfluidics technologies have allowed for the precise handling of the fluids and the dynamical stimulation at the sub-second scale and have been widely used to perform neuronal activity recordings in controlled experimental conditions improving high-throughput and automation.[7,8]

Most of calcium imaging experiments with chemical stimulation are nowadays carried out using microfluidics devices to spatially and temporally control the environment[9–11] while recording neuronal activity from olfactory neurons. One of the most successful microfluidic platforms for assaying chemosensory neuronal activity is the olfactory chip developed by Chronis et al.,[8] widely used to reveal stimulus-response relationships of chemosensory neurons in mechanically trapped nematodes. Larsch et al.[7] have developed microfluidic arenas to simultaneously record neuronal activity from about 20 nematodes at once by adopting wide-field fluorescence microscopy.

Nevertheless, in both microfluidic devices cited above, the chemical stimulus is delivered via a fluid flow controlled by valves that may induce the activation of some unwanted mechanosensitive processes, for example, ion channels involved in mechanosensation.[12] In fact, when the worm is loaded in a microfluidic device for olfactory stimulation, it is subject to a flowing stream that alternately contains the control or stimulus solution. In this condition, the nematode may experience the

D. Caprini, S. Schwartz, E. Lanza, E. Milanetti, G. Ferrarese, M. Nicoletti, V. Folli
Center for Life Nano- and Neuro-Science
Istituto Italiano di Tecnologia
Viale Regina Elena 291, Rome 00161, Italy
E-mail: davide.caprini@iit.it
E. Milanetti
Department of Physics
Sapienza University of Rome
Piazzale Aldo Moro 5, Rome 00185, Italy
V. Lucente
CREST OPTICS S.p.A.
Via di Torre Rossa 66, Rome 00165, Italy
G. Ferrarese, L. Chiodo, M. Nicoletti
Department of Engineering
Campus Bio-Medico University
Via Álvaro del Portillo 21, Rome 00128, Italy

The ORCID identification number(s) for the author(s) of this article can be found under https://doi.org/10.1002/adbi.202100927.

DOI: 10.1002/adbi.202100927

effect of both the hydrostatic pressure and the mechanical force of the flowing fluid. The latter comprises two components: the shear stress (the tangential component) and the pressure stress (the orthogonal component), both related to the velocity of the fluid. The opening/closing of valves controlling the delivery of the fluids will generate a transient perturbation of both the fluid velocity and hydrostatic pressure. This could potentially activate mechanosensitive neurons, therefore inducing spurious responses. In fact, mechanosensitive receptors could sense different types of mechanical stimuli like shear stress, tension, pressure, and osmotic stimuli.[13–15]

To investigate the characteristics of the nematode neuronal response upon mechanical stimulation in a microfluidic chip, we designed an innovative device with the microfluidic network divided, by grid slits, into two compartments, the main chamber and the side chamber. The fluid flows in the main chamber while the nematodes are loaded into the side chamber, where a flow free zone (stagnation area) is created. In this area, the velocity of the fluid can be more neglected the further the distance from the main chamber increases. The contribution of the flow force inside the stagnation area is minimal while the hydrostatic pressure (and its variation) continues to be present. Hence, such a device is designed to disentangle the effect of the mechanical stress and the hydrostatic pressure on neuronal activation.

In this study, this platform is used to investigate the effect of the mechanical stress on the activation of the Amphid wing "C" cells - ON (AWC^{ON}) neuron. AWC are olfactory neurons with winged cilia and are mainly involved in the sensation of volatile molecules.[9,16] There is abundant knowledge about the typical response of AWC neurons to a large class of chemicals, based on laser ablation,[17] calcium imaging,[9] and electrophysiology experiments.[18] In addition, AWC neurons have been also implicated in regulating thermosensory behaviors[19,20] and in controlling electrosensory navigation.[21,22]

Here, an unprecedented role of AWC^{ON} neuron in sensing temporal variation of the mechanical stress was detected. It was observed that AWC^{ON} neuron calcium activity is mainly correlated to the shear component of the mechanical stress due to the fluid stream.

A map of the mean activity of AWC^{ON} as a function of nematodes' position and head angle in the stagnation chamber is reported, highlighting a relationship between the head orientation and the flow direction.

The mechanically-induced activation of AWC^{ON} is preserved even in mutants defective for synaptic transmission. The results suggest that the mechanosensitivity of AWC^{ON} is an intrinsic property of the neuron rather than a consequence of inputs or feedback from the network. The calcium transient response requires the activity of the abnormal chemotaxis protein 4 (TAX-4) cyclic guanosine monophosphate (cGMP)-gated cation channel. In *tax-4* null mutants, all the mechanically-induced responses are eliminated. These results support a model in which the G protein–cGMP signaling is the main mediator of such mechanosensitivity, implicating the possible involvement of one or more odor receptors in the mechanotransduction of AWC^{ON}. Finally, it is found that the AWC^{ON} calcium events show a neuronal regime structurally different from the typical shape of the chemical response. The responses resemble a bistable dynamics,[23] in which the neurons can be switched from one stable state to the other by a transitory synaptic event. These findings suggest that distinct sensory strategies and signaling may be adopted from the neuron to respond to both chemical and mechanical stimuli.

2. Results

To evaluate the mechanical stresses on AWC^{ON} induced by the fluid flowing through the microfluidic device, we measured the neuron activation via calcium imaging of the GCaMP5a transgenic strain. We recorded calcium dynamics in AWC^{ON} neuron simultaneously from multiple nematodes by using a custom-made inverted fluorescence microscope at low magnification with a large numerical aperture objective (4×/0.28 N.A.).

Two different microfluidic devices are used, as detailed below, to highlight specific flow effects on the nematodes. The fluid supply was delivered via fluidic valves that control the inlet fluid in the device by the opening and the closing between two mutually exclusive buffer reservoirs. The switch between one reservoir or the other causes a temporal perturbation in the fluid velocity and in the hydrostatic pressure of the order of milliseconds due to the pinching action of the valves on the tubing (see Supporting Information). The time interval between valve switches may be selected according to a defined temporal pattern.

2.1. The AWC^{ON} Neuron Responds to Mechanical Stimulus upon Electrovalves Functioning

We first examined the AWC^{ON} activation for animals loaded in the mini-pulse arena, which is a downsized version of the pulse arena[24] with a recording chamber of 3×3 mm^2 (**Figure 1**A). The stimulation protocol is based on alternating the opening and closing of the two electrovalves. Nematodes were subjected to a 7 s long buffer pulse from reservoir "1" (valve "1" open, valve "2" closed), followed by a 25 s buffer pulse from reservoir "2" (first switch: valve "1" closed, valve "2" open), and to a 20 s buffer pulse from reservoir "1" (second switch: valve "1" open, valve "2" closed). So, each cycle of stimulation included two valve switches.

For our analysis, we selected nematodes with different head orientations (Figure 1B) accounting for the possibility that the neuronal activation may depend on the head position relative to the flow direction. The integration window for each head was of 10×10 pixels (Figure 1C). In Figure 1D, we report four representative responses from our sample, showing two opposite dynamics of intracellular calcium (hyperpolarization or depolarization). The neuronal responses show both a regime resembling a plateau activity as well as the typical shape of the chemosensory response, characterized by a faster decay. At increasing cycles number (Figure 1E,F), the frequency and the phase of the calcium signal did not change and the response strictly followed the applied stimulus. Here, we intend as plateau activity a prolonged and constant calcium response that can be triggered and terminated by a stimulus, in our case, the mechanical stimulation.

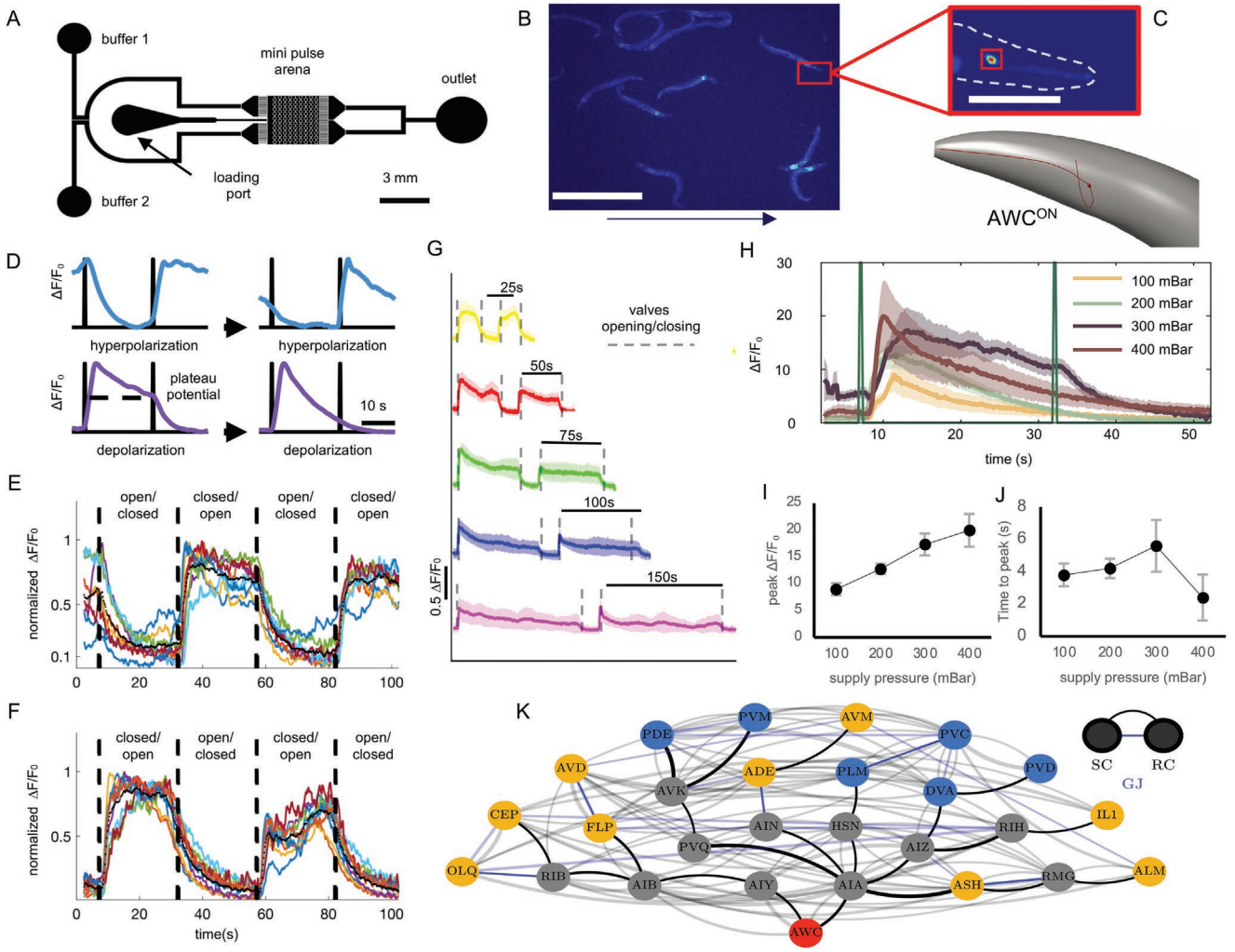

Figure 1. Wide-field imaging of neural activity and supporting microfluidic device used to show that AWC^{ON} neuron senses mechanical stimulus. A) Top view showing mini-pulse arena geometry. B) Cropped-frame camera images showing animals expressing GCaMP5 in AWC^{ON} neuron. (Scale bar, 1 mm). The black arrow indicates flow direction. C) Magnified view of the head from animal in (B). The red box on the neuron indicates the ROI for the numerical integration of pixel intensity (scale bar, 50 µm). D) Characteristic valve switch-evoked AWC^{ON} calcium transients displaying both hyperpolarizing and depolarizing behaviors. Each black line represents the opening of a valve and the closing of the other, and vice versa. E,F) AWC^{ON} sensory neuron responses during repeated mechanical stimulation through opening/closing of two electrovalves (dashed lines) for $n = 8$ and $n = 9$ animals, respectively (the response of each animal is represented as a colored line, black line is the mean across animals). The first switch can induce both an hyperpolarization and a depolarization. The waveforms differ not in frequency but only in phase (E,F), and can be superimposed considering a shift in time of half a cycle. G) Mean AWC^{ON} fluorescence response to systematic increase in the time interval between two valves switch (open/closed interval followed by closed/open interval) from 25 to 150 s with a supply pressure of 150 mBar. The shading represents ±1 s.e.m. and the signals are obtained averaging responses over $n = 39$ (at 25 s), $n = 28$ (at 50 s), $n = 22$ (at 75 s), $n = 42$ (at 100 s), $n = 20$ (at 150 s). H) Mean AWC^{ON} fluorescence response to systematic increase in the supply pressure selected through the manometer from 100 to 400 mBar. The shading represents ±1 s.e.m. and the signals are obtained averaging responses over seven animals. I,J) Mean AWC^{ON} peak fluorescence and time of response peak are influenced by the supply pressure in Figure 1H. K) The shortest paths from mechanosensory neurons to AWC neurons, excluding sensory neurons along the path.

The phase displacement among the responses from different neurons, reported in Figure 1E,F, can be explained by hypothesizing the presence of two stable neuronal states. To test this hypothesis, animals were subjected to a systematic increase in the time interval between two valves switches (open/closed interval followed by closed/open interval) from 25 to 150 s, at a supply pressure of 150 mBar (Figure 1G). The mechanical perturbation due to the instantaneous opening/closing of the valves induced a post-stimulus depolarized state that is maintained until a new mechanical perturbation was applied. Therefore, our results indicate that two stable states of intracellular calcium exist in AWC^{ON} neurons. The bistable regime in the calcium dynamics in AWC^{ON} is characteristic of mechanosensory responses and is not observed in their chemosensory responses.[9] However, this bistability in the calcium dynamics does not guarantee the existence of two stable states of the membrane potential that may eventually be tested with dedicated experiments.

To understand if the amplitude of the neuronal response was proportional to the intensity of the triggering stimulus,

we recorded neuronal responses to two repeated valve switches (one cycle) of increasing values of the supply pressure, from 100 to 400 mBar (Figure 1H). To analyze this effect, we select neurons undergoing a depolarization upon the first valve switch, because the two different waveforms (Figure 1E,F), differing not in frequency but only in phase, can be superimposed by a time shift of half a cycle, providing the same results.

Calcium levels of AWC^{ON} increased with the intensity of the supply pressure in a linearly dependent mode (Figure 1I). Pressure-response curves yielded peak fluorescence values that doubled in intensity from 100 to 400 mBar and the initial slope of the rising edge was also influenced by the amplitude of the mechanical stimulus (Figure 1I,J). Thus, AWC^{ON} sensory neuron dynamics reflects the amplitude of the applied stimulus. The calcium response observed in the soma of AWC^{ON} could be the result of inputs or feedback from other neurons (Figure 1K), or the effect of an intrinsic sensitivity of AWC^{ON} itself.

2.2. The AWC^{ON} Neuron Responds to Mechanical Stimulus upon Smooth Pressure Variations

Before analyzing the intrinsic or extrinsic nature of mechanosensing in AWC^{ON}, we studied the neural activation upon a different stimulation regime. We removed the electrovalves, whose activation (on the time scale of ≈10 ms) induces a shock wave causing an abrupt variation of both hydrostatic pressure and fluid velocity. We directly tuned the supply pressure with a manometer obtaining a smoother pressure variation, and we performed two kinds of experiments using only one inlet for buffer delivery.

In the first experiment, nematodes were subjected to laminar flow of the neutral buffer under a steady pressure increase (from 100 to 400 mBar in 200 s) as reported in **Figure 2**A–C. In the second experiment, we applied a stepwise pressure increase with each step being 50 s long (Figure 2D–F). Figure 2A shows fluorescent signals from 29 nematodes. Agglomerative cluster analysis on signal shapes revealed that responses may be categorized in three classes with a silhouette value of ≈0.7. Occurrence percentages of each class are reported in Figure 2B and their averaged shapes are shown in panel C. The same procedure has been applied to the step-wise pressure experiment (Figure 2D–F). In response to the linear ramp, the majority of signals showed a graded depolarization (blue curves), linearly dependent on the mechanical input. Few responses showed the opposite behavior corresponding to a graded hyperpolarization linearly dependent on the pressure (gray curves), while the minority of them seemed to be associated with a lack of response (red curves). In the stepwise experiment (Figure 2D–F), the majority of signals displayed a slow oscillation starting with a high hyperpolarization followed by a broad depolarization not clearly related to the triggering stimulus (blue curve in panel F reports the averaged response). Few responses showed depolarization followed by a plateau (red curve) while the minority of them displayed a slow hyperpolarization throughout the experiment (gray curve).

A possible interpretation of both experiments may be the presence of two stable states in the resting potential of AWC^{ON} neuron with different occurrence probabilities. Although this phenomenon has to be further characterized with targeted experiments, it is clear that this observed activity of the AWC^{ON} neuron is depending on mechanical stimuli delivered by flow changes even without shock waves-inducing fluidic valves.

2.3. The AWC^{ON} Mechanosensory Response is Intrinsic

Two possible scenarios may explain the observed AWC^{ON} response to mechanical stimulation: either AWC^{ON} is mechanosensitive, or it is part of the neural circuit activated by pressure variations. In the first case, the neuron must express some mechano-activated proteins. In the second one, the mechanical stimulus is sensed by a circuit involving mechanosensory neurons that recruit AWC^{ON} neuron as an interneuron, eliciting a change in its state of activity. In both cases, the neuronal activity recorded in the AWC^{ON} chemosensory neuron under mechanical stimuli is a novel and unforeseen ability.

To understand whether the observed calcium events are triggered by the stimulation of other presynaptic neurons or AWC^{ON} directly respond to mechanical stimuli, we analyzed calcium responses of two mutants, *unc-13* and *unc-31*, which are defective in communication through glutamate and neuropeptides, respectively.[25,26] Given that AWCs are glutamatergic and peptidergic,[27] these neurons are mildly decoupled from the rest of the nervous system in *unc-13* and *unc-31* mutants, ruling out the possible recruitment of AWC^{ON} into the mechanosensory circuit.

We found that AWC^{ON} responses in *unc-31* and *unc-13* mutants were not significantly different from the wild-type at 100 mBar (low supply pressure) (Figure 2G,H). Notably, mutant animals fail to respond to 300 mBar supply pressure with the same intensity as wild-type, suggesting that at higher pressures, an additional sensing mechanism comes into play (for example, inputs or feedback from other neurons responding only to intense pressure variations). Because these mutants express a different genetically encoded calcium indicator (GCaMP2.2b) with respect to the wild-type strain (GCaMP5), their relative fluorescence traces were re-scaled to account for the difference in fluorescence intensity. Together, these results suggest that the AWC^{ON} neuron senses mechanical stimuli, but the underlying molecular mechanism of sensory transduction is unclear. Some possible mechanisms are hypothesized below.

C. elegans ciliated mechanosensory neurons rely on a combination of degenerin/ephitelial sodium channel (DEG/ENaC) and transient receptor potential (TRP) channels to respond to mechanical stimuli.[28,29] AWC expresses only a TRPV (Vanilloid)-related ion channel, osmotic avoidance abnormal (OSM-9), which is demonstrated to have a role in mechanosensation.[30,31] However, genetic studies[32,33] showed that the expression of OSM-9 on the sensory cilia always requires the expression of an OCR protein. AWC does not express an OCR protein and OSM-9 is localized in the soma.[32] Hence, OSM-9 may not be involved in the response of this neuron to mechanical stimuli. Calcium traces of AWC^{ON} neuron in wild-type animals and *osm-9* mutants show similar dynamics both in response to chemical and mechanical stimuli, confirming that *osm-9* is

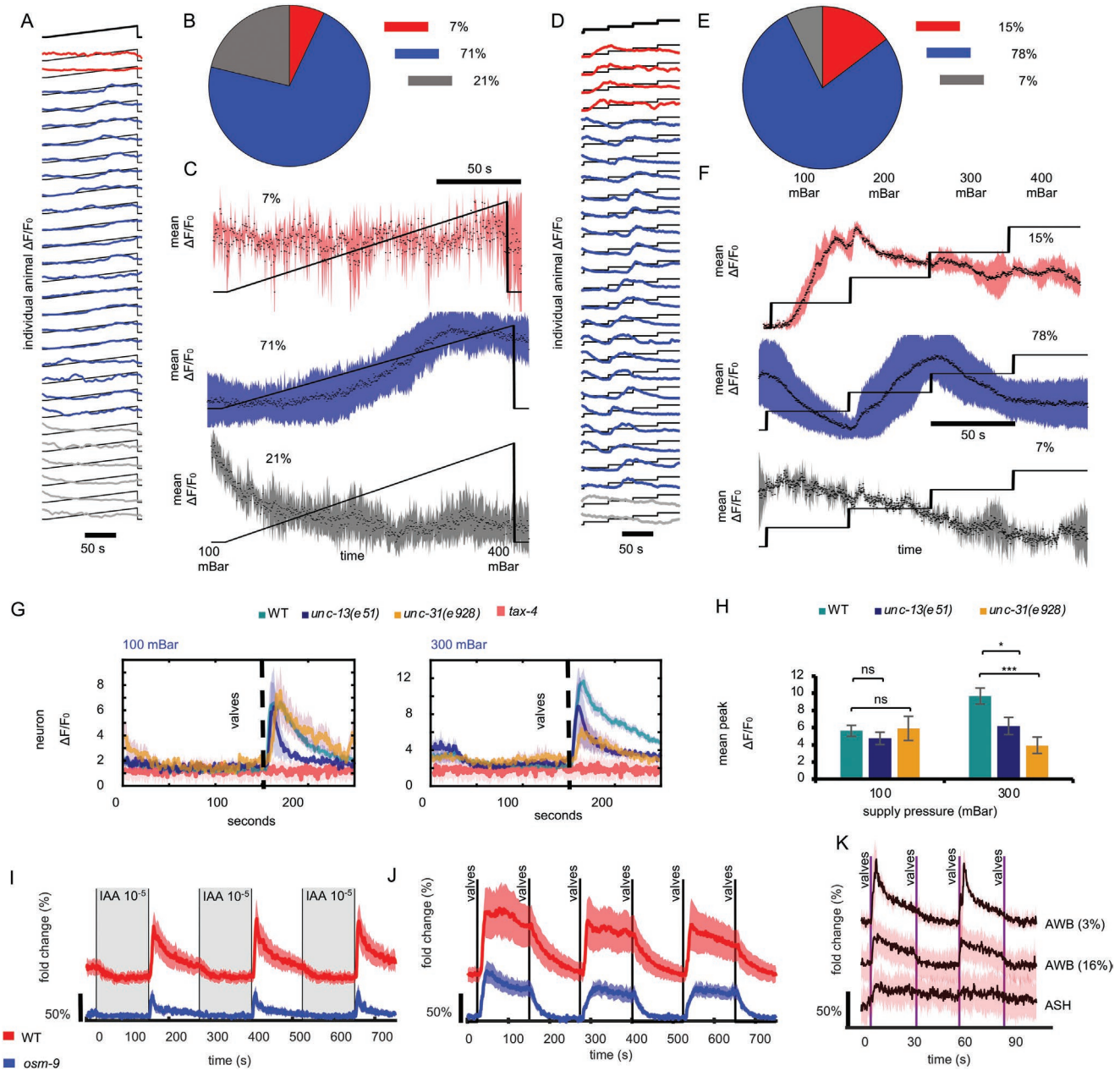

Figure 2. Pressure modulation of neuronal responses of AWC^{ON} neuron in the mini-pulse arena. A) Animals were subjected to a linear ramp of entrance pressure from 100 to 400 mBar in 200 s. Each curve represents the response of an individual animal. B) Agglomerative hierarchical cluster analysis on the data set composed by temporal traces of 29 individuals in (A) allows to separate curves in three clusters corresponding to three different neuronal responses. C) Average responses of neuronal activity of traces belonging to each cluster. The 71% of responses shows an increase in neuronal activity strongly correlated with the increasing pressure stimulus. The 7% of nematodes does not respond to pressure while the 21% of responses are anticorrelated with the stimulus. D) Stepwise pressure evoked fluorescence traces from 29 animals, E) agglomerative data analysis, and F) averaged responses. G) Intracellular calcium signals in mutants with defects in synaptic vesicle release *unc-13* and *unc-31* and mutants with defects in cGMP-dependent signaling *tax-4* compared to traces of wild-type animals. In each panel, traces indicate the mean normalized fluorescent traces averaged over $n \geqslant 5$ animals; the shading represents ±1 s.e.m. H) Mean AWC^{ON} peak fluorescence in WT, *unc-13* and *unc-31* mutants. At low pressure (100 mBar), there is no significant difference in response between the wild-type animals and mutants. At higher supply pressure, mutants responses have a smaller magnitude compared to wild-type animals. These results suggest that AWC^{ON} receives inputs from some mechanically-activated circuit that plays an additional role in the transient calcium increase of the AWC^{ON} neuron at higher pressure. (*$p \leqslant 0.05$, **$p \leqslant 0.001$, ***$p \leqslant 0.5$. I,J) Mean fluorescence fold change ($n > 10$ animals) of AWC^{ON} neuron in wild-type (red curve) and in *osm-9* mutant (blue) in response to chemical (I) and mechanical stimuli (J). K) ASH (n=18 animals) and AWB sensory neuron responses during mechanical stimulation through opening/closing of two electrovalves (vertical lines). The majority of AWB neurons did not respond (n = 113, not shown), a small percentage showed responses similar to AWC^{ON} neurons with two different decay times (n = 22, 16%, and n = 4, 3%). Signals from ASH neurons are noisy and not clearly correlated with the stimulation pattern.

not involved in mechanosensation (Figure 2I,J). Moreover, AWC expresses homologues of different types of voltage-gated channels (VGCCs)[34] that have been reported to be mechanosensitive.[35–37] The only *C. elegans* VGCC found to play a role in mechanosensation is EGL-19 by amplifying touch-evoked responses in anterior lateral microtubule cells (ALM) neurons.[38] To the best of our knowledge, the mechanosensitive properties of *C. elegans* egg Laying defective (EGL-19) have not yet been tested with dedicated electrophysiological studies, and there is no report of their expression in the AWC ciliary structure. As a consequence, although it is unlikely that EGL-19 are the primary sensors of the mechanical stimuli, they could play a role in the transduction of the mechanical stimuli by shaping calcium and voltage responses of AWC neurons.

An alternative mechanism responsible for inducing AWC^{ON} activation in response to mechanical stimuli would involve the G-protein coupled receptors (GPCRs) and their capacity to sense membrane stretch.[39–41] AWC^{ON} expresses several G-protein coupled receptors.[42,43] A potential signal transduction pathway for mechanical force detection in AWC^{ON} may involve the following components: G protein-coupled receptors (GPCRs), G-like proteins, receptor guanylate cyclases, and the cGMP-gated channel. Mechanical forces acting on cell membranes would increase the membrane tension and a consequent stretch detected by one or more specialized GPCRs. These membrane proteins activate G-like proteins that in turn regulate cGMP production by receptor-like guanylate cyclases. cGMP mediates the opening of the cGMP-gated channels encoded by *tax-2* and *tax-4* to depolarize the cell.[3]

As a preliminary test to determine whether the mechanical sensitivity of AWC^{ON} is potentially mediated by the GPCR signaling cascade, we used *tax-4* deletion mutants. We observed that the AWC^{ON} neuron did not respond to both low and high supply pressure (Figure 2G). These results support a model in which AWC^{ON} responses to mechanical stimuli are mediated by cGMP signaling and the increase of intracellular calcium depends on a mechanically-activated molecular pathway including TAX-4 and involving GPCRs activation.

2.4. Minimal Role of AWB and ASH Neurons in Mechanotransduction

Supporting a model in which mechanosensitivity is sustained by the GPCR signaling cascade, we wondered whether other olfactory neurons may be involved in sensing temporal variations in the fluid flow. We tested amphid neurons, single ciliated endings (ASH), a nociceptive neuron known to be also mechanosensitive, and amphid wing "B" cells (AWB), a winged olfactory neuron as AWC. Both neurons show calcium increases in response to variations in the fluid velocity caused by the valve (Figure 2K) but the responses are less robust and reliable than those recorded in AWC^{ON} neurons. A weak increase in intracellular calcium was recorded in ASH neurons at the first valve switch but the signal did not change significantly in response to subsequent switches. AWB neurons did not respond in the majority of the cases (81%). However, a small percentage (19%) of the traces showed responses similar to the ones of AWC^{ON} neurons with different decay times, alternating according to the valve switches.

2.5. Design of the Flow Free Chamber

A microfluidic device was developed by designing a geometry that enables to isolate the effect of the hydrostatic pressure from the mechanical forces associated with the fluid velocity (**Figure 3**A). Additionally, the proposed geometry can be used to deliver chemical stimulation avoiding interference due to the fluid flow. The device comprises a main chamber hosting an inlet and an outlet for liquid in- and out-flow respectively (Figure 3A) and it is designed to channel the fluid in a longitudinal direction. The main chamber is connected via multiple openings to the stagnation chamber where a population of nematodes (up to 25) is hosted. The openings are located at the interface between the main chamber and the stagnation chamber and do not alter the direction of the flow into the microfluidic device. The ratio between the cross-section of the main chamber and the cross-section of the inlet/outlet channels is greater than one.

A simulation conducted to evaluate the effect of an impulse inducing a perturbation in the fluid demonstrates that this geometry allows to create an environment, the stagnation chamber, in which the mechanical stress produced by the flow of the fluid is negligible (Figure 3B) with respect to the one produced in the mini-pulse arena (see Figure S2C,D, Supporting Information). The flow of the liquid passing through the device barely diverts inside the stagnation chamber, being confined in the main chamber. At the same time, the openings, while maintaining the continuity of the streamlines of the flow, allow the pressure perturbation associated with its flow to still reach the interior of the stagnation chamber. Figure 3C reports a simulation of the temporal trend of the hydrostatic pressure reflecting the square wave pulse comparable with the action of the fluidic solenoid valve.[44] The pressure reaches the asymptotic value of the steady state in short times (<0.05 s). The values of the pressure inside the two side chambers are nearly the same. The velocity perturbation instead (Figure 3D) has an important contribution only in the main chamber, both in the transient regime and in the steady state while being negligible in the stagnation area. This results in a strong reduction of mechanical stress. The grid slits between the two areas have a fundamental role in avoiding the propagation of the mechanical stress variation to the nematodes when they are confined in the stagnation chamber.

In this regard, a parametric analysis was conducted to define the optimal size of the slits (for more details, see Supporting Information). Their size has to ensure both the confinement of mechanical stress in the main chamber and the rapid diffusion of chemical substances inside the stagnation chamber. The simulations showed that by reducing the size of the openings, the fluid velocity variation into the stagnation chamber was greatly reduced (Figure S3, Supporting Information). A 50% ratio between openings and closings is the optimal trade-off between a strong reduction of the shear and fast propagation of chemicals in the stagnation area. In this configuration, the administration of chemical stimuli is guaranteed by diffusion and the stagnation chamber is fully filled up in tenths of a second at each switch of the fluidic valves (Figure 3E).

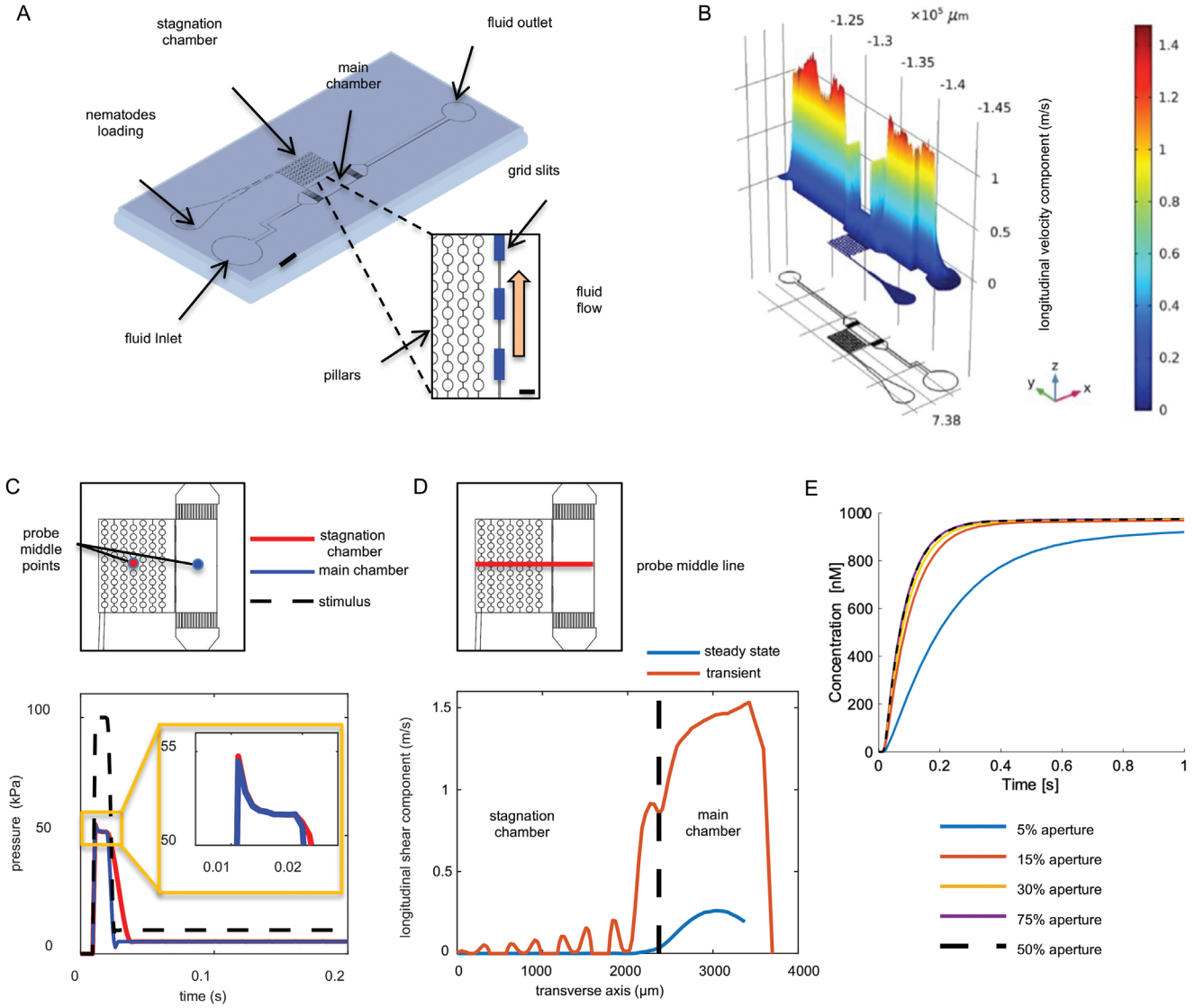

Figure 3. The "stagnation chip" for eliminating the tangential stress of the flowing fluid in the worms arena. A) The microfluidic chip consists of two communicating side chambers loaded with the fluid through the inlet. The inlet of the microfluidic channel is connected via polyethylene tubing and valves to the buffer reservoir and/or to a stimulus reservoir (depending on the experimental protocol). Video acquisition, pulse illumination, and fluidic valves for chemical/mechanical stimulation are computer-controlled and synchronized. The wide-field imaging at low magnification allows for multiple trace recordings (Scale bar, 2 mm). The insert shows a magnified view of the interface between the two arenas. The fluid flows in the main chamber and diffuses in the stagnation chamber through the grid slits. The microposts are present only in the stagnation chamber hosting the nematodes (Scale bar, 300 μm). B) Overview of steady state velocity magnitude in axial direction in the microfluidic structure. The design minimizes flow velocity changes during stimulation and, in the stagnation chamber, the shear velocity stress is nearly canceled (for the comparison with the standard mini-pulse arena, see Figure S2, Supporting Information). C) Temporal evolution of pressure stress measured in the middle point of the stagnation chamber (red line) and in the middle point of the main chamber (blue line) in response to a square wave pulse (dashed black line) applied at the inlet. D) Shear magnitude in a central section line of the microfluidic structure. The red line is the maximum shear change measured in the axial direction during the transient. The blue line is the value at the steady state. The dot vertical line indicates the position of the grid slits between the two side chambers. E) The temporal trend of the concentration of isoamyl alcohol measured in the middle point of the stagnation chamber and at different dimensions of the slits aperture. The percentage of opening of the slits is defined as the ratio of the sum of the slit lengths with respect to the total length of the interface wall between the two chambers. The diffusion process is faster as the percentage of openings increases. There is a significant reduction in the diffusion propagation for aperture ratio below 50%.

2.6. Study of the Shear-Dependent Neuronal Activity of AWC^{ON}

Our aim was to expose nematodes to repeated mechanical stimulation and investigate how the neuronal responses matched with the stimulation pattern and how they were affected by the position of the nematode in the stagnation area where a strong reduction of the mechanical stress is present. Buffer from reservoir "1" flowed for the first 10 s, while buffer from reservoir "2" flowed for the last 10 s. This cycle was repeated 20 times in each experiment. Numerical simulations showed

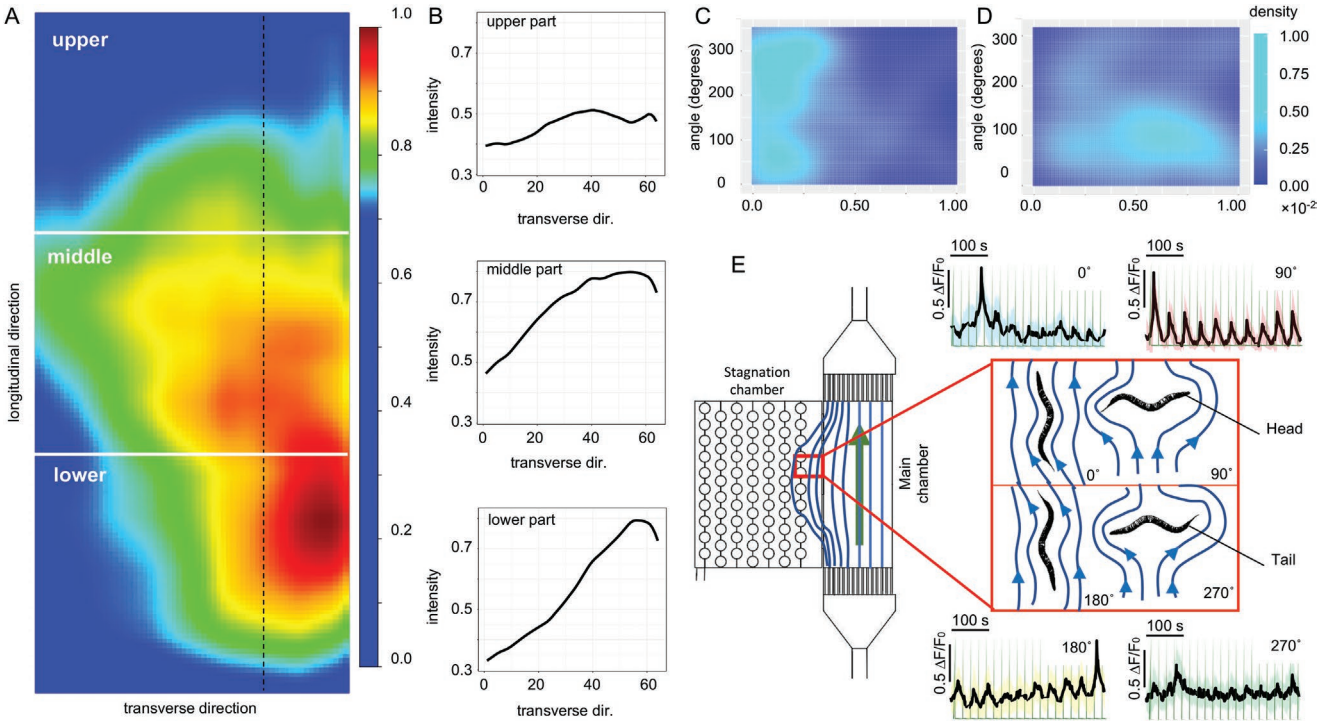

Figure 4. Mean activity of the AWC^{ON} neuron in the stagnation chamber. A) Smoothed average of the response intensity of multiple nematodes (271 trials with 116 animals) as a function of the position inside the stagnation chamber (sketch reported below). B) Intensity of the responses averaged along the longitudinal direction, reported from top to bottom as a function of the transverse direction for the upper, middle, and lower regions of the stagnation chamber, respectively. C) Probability density to record a given mean activity at a given angle considering the whole chamber. D) Probability density to record a given mean activity at a given angle considering only the region at the right side of the dotted line in (A), closer to the main chamber, where the recorded responses are associated with the highest intensities. E) The schematics represent the orientation of the nematode body inside the stagnation chamber with respect to the main flow direction. Mean AWC^{ON} fluorescence responses of nematodes oriented at 0°, 90°, 180° and 270° are also reported. The shading represents ± 1 s.e.m. and the signals are obtained averaging responses over n=11 (at 0°), n = 9 (at 90°), n = 12 (at 180°), and n = 12 (at 270°). 90° oriented nematodes showed responses strictly correlated with the pattern of stimulation (green lines represent the opening of a valve and the closing of the other).

how the fluid velocity decreases as a function of the distance from the main chamber (for more details, see Figure S3, Supporting Information). Notably, it is also reflected in the AWC^{ON} response. **Figure 4**A shows AWC^{ON} responses averaged over multiple nematodes as a function of the position in the stagnation chamber. The values of mean activity ranged from 0 (in this case, no nematode in that position responds to any cycle) to 1 (all nematodes in that position respond to all of the 20 cycles). Higher values are clustered close to the connection slits between the two chambers, where the velocity variation induced by the valve switches is less negligible (Figure 4B). These results suggest that AWC^{ON} neurons mainly sense fluid flow variations rather than variations in the hydrostatic pressure. Supposing that mechanical stress can be better sensed according to the orientation of the nematode heads with respect to the streamlines, we reported in Figure 4C the probability density to record a given intensity at a given angle (between head and streamlines). According to the data, low intensity responses are equally probable at any angle. However, focusing on the region associated with high intensity responses (right region of the dotted line in Figure 4A), we observed that the highest probability to record strong activity corresponds to a 90° angle of the head with respect to the streamlines (Figure 4D). In Figure 4E, the AWC^{ON} mean activity from $n \geqslant 10$ nematodes is reported for the main four angles formed by the head of the nematode with respect to the main flow direction (0°, 90°, 180°, and 270°). As also shown in panel D, 90° oriented nematodes showed the maximal activity with a significant variation in the intracellular calcium at every valve switch. At this orientation, the nematode head is pointed toward the grid slits and the sensitivity to variations in the fluid velocity due to the opening/closing of the valves is maximal. This is consistent with the hypothesis that the mechanical stress is mainly sensed through its shear (tangential) component in the AWC^{ON} neurons.

3. Conclusions

In the last years, microfluidics technologies have been applied to *C. elegans* and have allowed to perform neuronal recordings in controlled experimental conditions improving high-throughput and automation. However, the micro-environments experienced by the nematode in a microfluidic device can strongly affect its behavior and neural activity, like a microfluidic-induced sleep-state.[45]

In particular, a nematode in a microfluidic device is subjected to specific mechanical stimuli induced by the surrounding fluid: the hydrostatic pressure and the mechanical stress

associated with the velocity of the flowing fluid. The latter force has two components: the pressure stress (normal component) and the shear stress (tangential component), whose influence on the nematode may depend on its position and orientation with respect to the streamlines.

The use of valves to control the delivery of the fluids into the chip may introduce an additional perturbation in fluid velocity and hence in the mechanical stresses acting on the nematode. The effect of such perturbations on the worm behavior has not yet been characterized although they could elicit some mechanosensitive responses. In fact, the majority of studies on mechanosensation mainly referred to touch stimuli as localized indentation or compression.[15,46,47]

Herein, we provide a novel microfluidic device, which hosts an arena that minimizes the velocity perturbation induced by the use of valves. By decoupling the mechanical stress from the hydrostatic pressure, this device allows to investigate the role of shear and pressure stresses in evoking neuronal activation.

Apart mechanosensing dedicated neurons, it has been recently demonstrated that olfactory sensory neurons, in the mouse, are also sensitive to mechanical stimuli,[41,48,49] possibly relying on the same olfactory transduction cascade. This mechanosensation has been proved to promote a robust phase coding of odors,[50] enhancing the olfactory capabilities.

Despite similar effects have not yet been observed in nematodes, we have identified an olfactory neuron, AWC^{ON} that responds to the mechanical stimulus induced by a variation in fluid velocity. The dynamics of calcium events in response to such variation is not only correlated with the stimulus amplitude but it also depends on the previous activity state of the neuron. However, the origin of this dependence is not yet clear and has to be investigated at the molecular level. Moreover, we observe transitions between up and down states in calcium traces which can be triggered by the same perturbation in fluid velocity, suggesting an underlying bistable activity of the neuron. However, the latter hypothesis would need to be confirmed through patch-clamp experiments or the use of voltage sensitive dyes.

Tests with mutants defective in the release of the dense core (*unc-31*) and clear vesicles (*unc-13*) reveal that the synaptic transmission of AWC^{ON} neuron with inner circuits is not required for the mechanically-induced responses. This suggests that AWC^{ON} directly senses the mechanical stimuli either via ionotropic or metabotropic pathways and that the observed variability in shapes and timings of neuronal dynamics may be an intrinsic neuronal property related to the number and kind of the involved mechanosensory receptors.

As far as the ionic channels are concerned, a putative candidate could be the OSM-9 channel.[30,31] However, the lack of OCR proteins in AWC^{ON} impedes OSM-9 localization on the sensory cilia. As observed in ASH neurons,[32] this is an essential requirement for mechanosensation. Our results on *osm-9* mutants confirm that this calcium channel is not responsible for AWC^{ON} mechanosensitivity. Moreover, AWC does not express any other of the DEG/ENaC, TRP or PIEZO channels known to be involved in *C. elegans* mechanosensation.[29,46,51]

Considering the metabotropic pathways, an alternative hypothesis is the involvement of some G-protein coupled receptors. Indeed, GPCRs could sense different mechanical stimuli including fluid shear stress.[39,52,53] AWC neurons express more than 20 GPCRs,[42] and multiple G-proteins interacting with them. TAX-4 are cyclic nucleotide gated channels involved in several processes including G protein-coupled receptor signaling pathways. In our recordings for *tax-4* mutants, the mechanical responses are abolished. Such a result also works against the possibility that AWC^{ON} may receive mechanosensory signals from other neurons through gap junctions. A proper experimental characterization of the putative GPCR-mediated mechanotransduction would require an extensive study on mutants for all the GPCRs and the G-proteins, allowing the identification of the specific molecular mechanisms regulating the mechanotransduction. Future studies may investigate this hypothesis in AWC neurons, scrutinizing the interplay between mechanosensitivity and olfaction in *C. elegans*. Additionally, it would be worth exploiting whole-brain imaging to dissect alternative mechanosensitive circuits including AWC, and to determine how the signals from AWC neurons are processed through the circuit according to chemical and mechanical stimuli respectively.

To confirm the peculiarity of the AWC^{ON} mechanosensitivity, we tested other two neurons involved in odorsensation, AWB, and ASH. We obtained a scarce activation upon mechanical stimulation for AWB and a very weak, not well characterized, activation for ASH.

In conclusion, our findings show that the olfactory AWC^{ON} neurons sense mechanical stress and identify the G protein-cGMP signaling as the main mediator of such mechanotransduction, implicating the possible involvement of one or more odor receptors. Our results contribute to shed light on the molecular mechanisms underpinning the complex nature of the *C. elegans* polymodal sensory neurons. Moreover, the microfluidic platform we employ can be adapted for the study of cell cultures as well as for on-chip experiments in which preventing the influence of mechanical stimuli is a critical aspect. In fact, when working with microfluidic devices, the shear stress experienced by the cells is a fundamental factor to take into consideration. Indeed, the level of the shear stress may alter the physiological responses, possibly leading to cell damage, shape and density modifications, and altered cell signaling pathways. So, our device provides a solution for controlled-environment experiments in which the shear stress needs to be greatly reduced.

4. Experimental Section

Device Fabrication: The selected fabrication process had to ensure high optical quality and biocompability. Calcium imaging experiments were always conducted on devices made of polydimethylsiloxane (PDMS) on glass. Simulations performed on fluid consider the microfluidic chip as a rigid unit, neglecting the potential elastic effect of the polymer in the transient pressure. A stiff microchip which is also optically transparent, with no plastic material, would require complex glass bonding microfabrication techniques.[54,55] The microfluidic devices of PDMS on glass were prepared by using the soft lithography process.[56] The SU-8 (MicroChem 3000 series) structure was fabricated on a glass substrate by conventional photolithography to obtain a 50 microns thick monolayer microfluidic network. A high resolution photomask was directly printed on the microfluidic network with a laser writer to ensure a resolution under two microns for the smallest features. The 1:10 PDMS

(Silgard 184) mold replica was cured after the casting process and the holes for inlet/outlet were made with 0.6 mm puncher, allowing for connection with external 0.02 in. ID Tygon tubes. The PDMS layer was bonded on a microscope glass slider by using an air-plasma treatment (HARRIK PLASMA) and thermal recovery on a hot plate.

Experimental Set-Up and Stimulation: These experiments were carried out with two different microfluidic devices. The first one was a miniaturized and revised version of the pulse arena by Albrecht et al.,[24] here referred as "mini-pulse" (Figure 1B). The fluidic device was designed with inlet channels tailored to present temporal pulses of chemical substances via fluidic valves. The duration and the repetition rate of the chemical pulse were defined according to a programmed pattern. For this study, no chemical stimulus was provided by alternating opening and closing between two valves connected to two neutral buffer reservoirs (S Basal). In this device, nematodes were subjected to instantaneous changes in pressure and flow velocity at every opening/closing of the valves with an intensity depending on the supply pressure value fixed at the beginning of the experiment. The second device, the "stagnation chip", had a flow free zone designed to exclude the tangential mechanical stress in the chamber hosting the nematodes (see Section 2.5 and Supporting Information). For each device, several trials were performed and neuronal activity was recorded after the switch between the two buffer reservoirs. Both devices were placed on a custom designed inverted microscope. Bright-field imaging at 1.25× magnification was used during worms loading via PE tubing to visualize the entire arena and to ensure the proper arrangement of the worms in the stagnation chamber or in the mini-pulse arena. To record neuronal activation, fluorescence imaging was used to excite a genetically encoded calcium indicator (GCaMP5a) on AWC^{ON} at 470 nm. Excitation light was reflected on the sample from a high power LED (470 nm - M470L2, Thorlabs, Newton, New Jersey) with a FITC excitation filter (MF475-35, CWL = 475 nm, BW = 35 nm, Thorlabs) and a condenser (ACL2520U-A, Thorlabs) using a dichroic mirror (MD498, Thorlabs). Fluorescent signals were collected by a digital CMOS camera (ORCA-Flash4.0 C11440, Hamamatsu, Hamamatsu City, Japan) through the dichroic mirror with a pass-band FITC/TRITC filter (59004×, Chroma, Bellows Falls, Vermont) using a 4× objective with a numerical aperture of 0.28 (XLFLUOR4X/340, Olympus, Tokyo, Japan) for a field of view of (3.25×3.25 mm^2). During recordings, a transmission channel (illumination at 660 nm through a high power LED, M660L4, Thorlabs) allowed to select the visualized area of the arena through a motorized stage (MLS203-1, Thorlabs). To maximize resolution in time and to reduce phototoxicity, the excitation LED and the camera shutter were synchronized so that the arena was illuminated only during the exposure time (100 ms). To control fluid dynamics, a set of electrovalves was connected to the inlet reservoirs and the stimulus delivery was controlled via digital signals (from National Instruments controller NI-DAQmx (PCI-6221, National Instruments, Austin, Texas) to a VC-6 valve controller (Warner Instruments Corporation)). The whole setup was automatized by connecting the light emitting diodes (LEDs), the electrovalves and the camera to a PC (Windows 10, 64-bit, Microsoft, Redmond, Washington) through a National Instruments controller (PCI-6221, National Instruments, Austin, Texas). A custom-made software in MATLAB (Mathworks, Natick, Massachusetts) was used for synchronized illumination, image acquisition, fluid delivery control, and data recording.

Experimental Protocol: Before each experiment, the microfluidic chip was degassed in a vacuum bell for at least 15 min to prevent air bubbles from transferring from the PDMS into the chip. The outflow port was connected to the outflow reservoir. The loading inlet was used to completely fill the device with buffer solution (S Basal) until a droplet emerged from both inlets. Then, the two inlets were connected to the two reservoirs (buffer–buffer) using drop-to-drop connections. Both valves were open to flush the device with buffer solution for a few minutes while the loading inlet was blocked. Next, the loading tubing was used to gently inject ≈10–15 nematodes into the chip via syringe. The arena was flushed continuously for 10 min with buffer solution to remove any residual bacteria. The chip was filled with a solution of levamisole hydrochloride diluited in Milli-Q water. Levamisole was an acetylcholine receptor–specific agonist here used to paralyze the animal's muscles and reduce motion artifacts during the experiment. A motorized *xy*-stage allowed to move the device in the field of view of the camera and to verify the correct loading procedures. The exposition time of complementary metal–oxide–semiconductor (CMOS) camera was 100 ms and the excitation LED was activated in sync with the camera shutter after the first ten background frames. A pulsed LED illumination of 100 ms prevented photo-bleaching over long lasting and repeated experiments.

Data Analysis and Statistical Analysis: Neuronal traces were analyzed by using custom MATLAB scripts. Acquired images were pre-treated by subtracting a mean background averaged over 10 initial background frames, and by applying an averaging filter for noise reduction. A custom-made GUI allowed the user to select ROIs containing viable nematode heads at a reference frame. In each ROI, the user was required to select the position of the AWC^{ON} neuron. On the basis of this information, the script tracked neuronal positions throughout the video in both temporal directions by looking for the maximum intensity averaged over a 10×10 pixels area within 30 pixels from the neuronal position assigned in the previously processed frame. The normalized calcium response, $I(t)$, was calculated as $I(t) = \frac{\Delta F(t)}{F_0}$, where $F(t)$ is the fluorescence recorded at time t and $\Delta F(t) = F(t) - F_{\text{background}}$ is the background-corrected integrated neuronal fluorescent trace. The baseline value of fluorescence F_0 was evaluated as the mean of $\Delta F(t)$ for the first 5 s, a stimulus free time window, in which the neuron is quiescent. Normalized traces were averaged across 3–5 trials for each animal. To assess the response in the stagnation chamber, nematodes were stimulated with a series of 20 switches of the fluidic valves. Fluorescent traces were collected and the resulting mean activity of the AWC^{ON} neuron for nematode i at the position (x,y) in the chamber was evaluated through the quantity $A_i = n_p/n_c$, where n_p is the number of peaks of $I(t)$ and n_c, the number of stimulation cycles ($n_c = 10$). For the statistical analysis of the mean activity, the lattice of the stagnation chamber was schematized as a matrix, R, whose dimensions are $N \times M$, with $n = 31$ and $M = 23$. In each acquisition, each worm was identified with a number ranging from 1 to N_w, and N_w represented the total number of nematodes in the device. At time t, each nematode could occupy only one element of the R matrix. The average of the intensity value acquired during the experiments, was reported for each matrix element, defining the final matrix R_{av}. To better visualize the results, a smoothing procedure on the R_{av} matrix was adopted. Therefore, it was assigned to each matrix element of the R_{av} matrix, the average value calculated on the first N_s neighboring matrix elements (in this case $N_s = 1$). In order to perform an additional smooth procedure with a larger side of the square, the size of the matrix was increased. Therefore, each matrix element was mapped in a square of elements of matrix $L \times L$, thus increasing each side of the original matrix by a factor L (in this case $L = 5$). This matrix was called *RI*. Subsequently, a smooth procedure was adopted, replacing each element of the *RI* matrix with the average of the values belonging to a square of side 15 centered on the RI_{ij} element. In order to analyze the different intensity trends based on the acquisition region, the average signal was calculated in three regions of the same length (upper, middle, and lower part) along the vertical axis (longitudinal direction with respect to the flow) of the matrix, studying it in function of horizontal axis (transverse direction). Furthermore, the study of the orientation of each worm according to the response intensity values was performed. Since both the angle and the intensity were discrete values, which fill almost all the available space, the analysis was conducted in terms of density in the space of the two variables. The higher the level of the density value in a given region, the higher the probability of finding a worm with the corresponding angle and intensity values. In order to study the relation between the intensity variable and the orientation variable in the regions close to the flow of the current, the first N_{col} columns from the right of the matrix were considered (in this case $N_{col} = 10$). The analysis was performed using codes developed in-house. In Figure 2H, statistical analysis was performed with MATLAB using *t*-test to evaluate differences between WT animals and mutants. A value of $p \leqslant 0.05$ was considered statistically significant, ($*p \leqslant 0.05$, $**p \leqslant 0.01$, $***p \leqslant 0.001$).

C. elegans Maintenance and Reagents Preparation: Experiments were conducted using transgenic animals harboring the GCaMP fluorophore

in the AWC^{ON} sensory neuron. The strains used are: CX17256 *(kyIs722[str-2p::GCaMP5(D380Y) + elt-2::mCherry]*, VC3113 (*tax-4 (ok3771)*), and CX10 (*osm-9 (ky10)*), all obtained from the Caenorhabditis Genetics Center which is funded by NIH Office of Research Infrastructure Programs (P40 OD010440). *unc-13(e51) I; kyEx2595 [str2::GCaMP2.2b, unc-122::gfp]* and *unc-31(e928) IV; kyEx2595 [str2::GCaMP2.2b, unc-122::gfp]*, both kindly provided by Professor Chalasani (Salk Institute for Biological Studies, La Jolla, CA). Strains AWB and ASH were a kind gift from Dr. Zaslaver (The Hebrew University of Jerusalem). These strains were PS6384 (AWB) *syEx1245[str-1::GCaMP3+pha-1]; pha-1(e2123ts)* and PS6386 (ASH) *syEx1246[sra-6::GCaMP3+pha-1]; pha-1(e2123ts)*. The VC3113 and CX10 strains were genetically crossed to CX17256 strain to obtain *tax-4* and *osm-9* deletion mutants harboring the GCaMP5 fluorophore to perform calcium imaging experiments. Nematodes were cultured under standard conditions at 20 °C on nematode growth media (NGM) in 60 mm petri dishes seeded with *Escherichia coli* strain OP50 as a food source. Worms from the CX17256 strain were synchronized by placing 10 adult hermaphrodites on NGM plates for 4 h to lay eggs. The hermaphrodites were then removed and plates were placed in an incubator at 20 °C. The *unc-13* and *unc-31* mutants were instead collected directly from the culture plates since their rate of deposition was lower compared to that of CX17256 strain. The day of the experiment, 15–20 fluorescent adults were picked and placed in 35 mm petri dishes, washed three times with S-basal (NaCl 0.1 M, potassium phosphate 0.05 M, pH6) and injected into the microfluidic device. Animals were paralyzed inside the chip using levamisole hydrochloride (Sigma-Aldrich PHR1798) diluted in Milli-Q water at a final concentration of 1 mM. Isoamyl alcohol (Sigma-Aldrich 8.18969) was used as the chemical stimulus and diluted in S-basal buffer at a final 10^{-7} dilution.

Supporting Information

Supporting Information is available from the Wiley Online Library or from the author.

Acknowledgements

The authors thank the Caenorhabditis Genetics Center (CGC) for strains CX17256, CX10, and VC3113, S. H. Chalasani for *unc-13* and *unc-31* mutants, A. Zaslaver for strains PS6384 and PS6386, M. Di Rocco for assistance in performing genetic crosses, and E. Rondanina for providing high-resolution photo-masks. This work was funded by the CrestOptics S.p.A, Rome, Italy.

Open Access Funding provided by Istituto Italiano di Tecnologia within the CRUI-CARE Agreement.

Conflict of Interest

The authors declare no conflict of interest.

Data Availability Statement

Research data are not shared.

Keywords

AWC^{ON}, *Caenorhabditis elegans*, mechanosensation, microfluidics, pressure, shear stress

Received: June 18, 2021
Revised: August 3, 2021
Published online: August 22, 2021

[1] M. Chalfie, J. E. Sulston, J. G. White, E. Southgate, J. N. Thomson, S. Brenner, *J. Neurosci.* **1985**, *5*, 956.
[2] I. Mori, Y. Ohshima, *Nature* **1995**, *376*, 344.
[3] C. I. Bargmann, in *WormBook: The Online Review of C. Elegans Biology*, **2006**.
[4] E. Lanza, S. Di Angelantonio, G. Gosti, G. Ruocco, V. Folli, *Neurocomputing* **2021**, *430*, 1.
[5] E. R. Troemel, *Bioessays* **1999**, *21*, 1011.
[6] L. Tian, S. A. Hires, T. Mao, D. Huber, M. E. Chiappe, S. H. Chalasani, L. Petreanu, J. Akerboom, S. A. McKinney, E. R. Schreiter, C. I. Bargmann, V. Jayaraman, K. Svoboda, L. L. Looger, *Nat. Methods* **2009**, *6*, 875.
[7] J. Larsch, D. Ventimiglia, C. I. Bargmann, D. R. Albrecht, *Proc. Natl. Acad. Sci. U. S. A.* **2013**, *110*, E4266.
[8] N. Chronis, M. Zimmer, C. I. Bargmann, *Nat. Methods* **2007**, *4*, 727.
[9] S. H. Chalasani, N. Chronis, M. Tsunozaki, J. M. Gray, D. Ramot, M. B. Goodman, C. I. Bargmann, *Nature* **2007**, *450*, 63.
[10] K. Yoshida, T. Hirotsu, T. Tagawa, S. Oda, T. Wakabayashi, Y. Iino, T. Ishihara, *Nat. Commun.* **2012**, *3*, 739.
[11] A. Zaslaver, I. Liani, O. Shtangel, S. Ginzburg, L. Yee, P. W. Sternberg, *Proc. Natl. Acad. Sci. U. S. A.* **2015**, *112*, 1185.
[12] D. Bazopoulou, N. Tavernarakis, *Curr. Top. Membr.* **2007**, *59*, 49.
[13] S. Shi, C. J. Luke, M. T. Miedel, G. A. Silverman, T. R. Kleyman, *J. Biol. Chem.* **2016**, *291*, 14012.
[14] M. Nicoletti, L. Chiodo, A. Loppini, *Mathematics* **2021**, *9*, 323.
[15] A. L. Nekimken, H. Fehlauer, A. A. Kim, S. N. Manosalvas-Kjono, P. Ladpli, F. Memon, D. Gopisetty, V. Sanchez, M. B. Goodman, B. L. Pruitt, M. Krieg, *Lab Chip* **2017**, *17*, 1116.
[16] C. I. Bargmann, E. Hartwieg, H. R. Horvitz, *Cell* **1993**, *74*, 515.
[17] P. D. Wes, C. I. Bargmann, *Nature* **2001**, *410*, 698.
[18] D. Ramot, B. MacInnis, M. B. Goodman, *Nat. Neurosci.* **2008**, *11*, 908.
[19] A. Kuhara, M. Okumura, T. Kimata, Y. Tanizawa, R. Takano, K. D. Kimura, H. Inada, K. Matsumoto, I. Mori, *Science* **2008**, *320*, 803.
[20] D. Biron, S. Wasserman, J. H. Thomas, A. D. Samuel, P. Sengupta, *Proc. Natl. Acad. Sci. U. S. A.* **2008**, *105*, 11002.
[21] C. V. Gabel, H. Gabel, D. Pavlichin, A. Kao, D. A. Clark, A. D. Samuel, *J. Neurosci.* **2007**, *27*, 7586.
[22] S. D. Chrisman, C. B. Waite, A. G. Scoville, L. Carnell, *PLoS One* **2016**, *11*, e0151320.
[23] M. Nicoletti, A. Loppini, L. Chiodo, V. Folli, G. Ruocco, S. Filippi, *PLoS One* **2019**, *14*, e0218738.
[24] D. R. Albrecht, C. I. Bargmann, *Nat. Methods* **2011**, *8*, 599.
[25] J. E. Richmond, W. S. Davis, E. M. Jorgensen, *Nat. Neurosci.* **1999**, *2*, 959.
[26] S. Speese, M. Petrie, K. Schuske, M. Ailion, K. Ann, K. Iwasaki, E. M. Jorgensen, T. F. J. Martin, *J. Neurosci.* **2007**, *27*, 6150.
[27] S. H. Chalasani, S. Kato, D. R. Albrecht, T. Nakagawa, L. Abbott, C. I. Bargmann, *Nat. Neurosci.* **2010**, *13*, 615.
[28] S. L. Geffeney, M. B. Goodman, *Neuron* **2012**, *74*, 609.
[29] Y.-Q. Tang, S. A. Lee, M. Rahman, S. A. Vanapalli, H. Lu, W. R. Schafer, *Neuron* **2020**, *107*, 112.e10.
[30] R. G. O'Neil, S. Heller, *Pfluegers Arch.* **2005**, *451*, 193.
[31] H. A. Colbert, T. L. Smith, C. I. Bargmann, *J. Neurosci.* **1997**, *17*, 8259.
[32] D. M. Tobin, D. M. Madsen, A. Kahn-Kirby, E. L. Peckol, G. Moulder, R. Barstead, A. V. Maricq, C. I. Bargmann, *Neuron* **2002**, *35*, 307.
[33] J. M. Kaplan, H. R. HoRVITZ, *Proc. Natl. Acad. Sci. U. S. A.* **1993**, *90*, 2227.
[34] O. Hobert, in *WormBook: The Online Review of C. Elegans Biology*, **2013**.
[35] G. L. Lyford, P. R. Strege, A. Shepard, Y. Ou, L. Ermilov, S. M. Miller, S. J. Gibbons, J. L. Rae, J. H. Szurszewski, G. Farrugia, *Am. J. Physiol.: Cell Physiol.* **2002**, *283*, C1001.

[36] J. Hao, F. Padilla, M. Dandonneau, C. Lavebratt, F. Lesage, J. Noël, P. Delmas, *Neuron* **2013**, *77*, 899.
[37] C. E. Morris, E. A. Prikryl, B. Joós, *PLoS One* **2015**, *10*, e0118335.
[38] X. Chen, M. Chalfie, *J. Neurosci.* **2014**, *34*, 6522.
[39] S. Erdogmus, U. Storch, L. Danner, J. Becker, M. Winter, N. Ziegler, A. Wirth, S. Offermanns, C. Hoffmann, T. Gudermann, M. M. y Schnitzler, *Nat. Commun.* **2019**, *10*, 5784.
[40] M. Mederos y Schnitzler, U. Storch, T. Gudermann, *Microcirculation* **2016**, *23*, 621.
[41] T. Connelly, Y. Yu, X. Grosmaitre, J. Wang, L. C. Santarelli, A. Savigner, X. Qiao, Z. Wang, D. R. Storm, M. Ma, *Proc. Natl. Acad. Sci. U. S. A.* **2015**, *112*, 590.
[42] B. Vidal, U. Aghayeva, H. Sun, C. Wang, L. Glenwinkel, E. A. Bayer, O. Hobert, *PLoS Biol.* **2018**, *16*, e2004218.
[43] E. Milanetti, G. Gosti, L. De Flaviis, P. P. Olimpieri, S. Schwartz, D. Caprini, G. Ruocco, V. Folli, *Biophys. Chem.* **2019**, *255*, 106264.
[44] A. T. Lau, H. M. Yip, K. C. Ng, X. Cui, R. H. Lam, *Micromachines* **2014**, *5*, 50.
[45] D. L. Gonzales, J. Zhou, B. Fan, J. T. Robinson, *Nat. Commun.* **2019**, *10*, 5035.
[46] M. B. Goodman, *WormBook: The Online Review of C. Elegans Biology* **2006**, pp. 1–14.
[47] M. B. Goodman, P. Sengupta, *Genetics* **2019**, *212*, 25.
[48] X. Chen, Z. Xia, D. R. Storm, *J. Neurosci.* **2012**, *32*, 15769.
[49] X. Grosmaitre, L. C. Santarelli, J. Tan, M. Luo, M. Ma, *Nat. Neurosci.* **2007**, *10*, 348.
[50] R. Iwata, H. Kiyonari, T. Imai, *Neuron* **2017**, *96*, 1139.
[51] X. Bai, J. Bouffard, A. Lord, K. Brugman, P. W. Sternberg, E. J. Cram, A. Golden, *Elife* **2020**, *9*, e53603.
[52] J. Xu, J. Mathur, E. Vessières, S. Hammack, K. Nonomura, J. Favre, L. Grimaud, M. Petrus, A. Francisco, J. Li, V. Lee, F.-L. Xiang, J. K. Mainquist, S. M. Cahalan, A. P. Orth, J. R. Walker, S. Ma, V. Lukacs, L. Bordone, M. Bandell, B. Laffitte, Y. Xu, S. Chien, D. Henrion, A. Patapoutian, *Cell* **2018**, *173*, 762.
[53] M. Chachisvilis, Y.-L. Zhang, J. A. Frangos, *Proc. Natl. Acad. Sci. U. S. A.* **2006**, *103*, 15463.
[54] J. Hwang, Y. H. Cho, M. S. Park, B. H. Kim, *Int. J. Precis. Eng. Manuf.* **2019**, *20*, 479.
[55] D. Caprini, A. Nascetti, G. Petrucci, D. Caputo, G. de Cesare, in *2015 XVIII AISEM Annual Conf.*, IEEE, Piscataway, NJ **2015**, pp. 1–4.
[56] D. Qin, Y. Xia, G. M. Whitesides, *Nat. Protoc.* **2010**, *5*, 491.